AEDC-TR-75-118

cy.2

CALCULATION OF THE BOUNDARY-LAYER GROWTH IN A LUDWIEG TUBE

VON KÁRMÁN GAS DYNAMICS FACILITY
ARNOLD ENGINEERING DEVELOPMENT CENTER
AIR FORCE SYSTEMS COMMAND
ARNOLD AIR FORCE STATION, TENNESSEE 37389

December 1975

Final Report for Period July 1973 — December 1974

Prepared for

DIRECTORATE OF TECHNOLOGY (DY)
ARNOLD ENGINEERING DEVELOPMENT CENTER
ARNOLD AIR FORCE STATION, TENNESSEE 37389

APPROVAL STATEMENT

This technical report has been reviewed and is approved for publication.

FOR THE COMMANDER

Carlos Tirres

CARLOS TIRRES
Captain, USAF
Research & Development Division
Directorate of Technology

Robert O. Dietz

ROBERT O. DIETZ
Director of Technology

UNCLASSIFIED

REPORT DOCUMENTATION PAGE		READ INSTRUCTIONS BEFORE COMPLETING FORM
1. REPORT NUMBER AEDC-TR-75-118	2. GOVT ACCESSION NO.	3. RECIPIENT'S CATALOG NUMBER
4. TITLE (and Subtitle) CALCULATION OF THE BOUNDARY-LAYER GROWTH IN A LUDWIEG TUBE		5. TYPE OF REPORT & PERIOD COVERED Final Report-July 1973 - December 1974
		6. PERFORMING ORG. REPORT NUMBER
7. AUTHOR(s) James C. Sivells, ARO, Inc.		8. CONTRACT OR GRANT NUMBER(s)
9. PERFORMING ORGANIZATION NAME AND ADDRESS Arnold Engineering Development Center (DY) Arnold Air Force Station, Tennessee 37389		10. PROGRAM ELEMENT, PROJECT, TASK AREA & WORK UNIT NUMBERS Program Element 65807F
11. CONTROLLING OFFICE NAME AND ADDRESS Arnold Engineering Development Center (DYFS) Arnold Air Force Station, Tennessee 37389		12. REPORT DATE December 1975
		13. NUMBER OF PAGES 36
14. MONITORING AGENCY NAME & ADDRESS(if different from Controlling Office)		15. SECURITY CLASS. (of this report) UNCLASSIFIED
		15a. DECLASSIFICATION/DOWNGRADING SCHEDULE N/A

16. DISTRIBUTION STATEMENT (of this Report)

Approved for public release; distribution unlimited.

17. DISTRIBUTION STATEMENT (of the abstract entered in Block 20, if different from Report)

18. SUPPLEMENTARY NOTES

Available in DDC

19. KEY WORDS (Continue on reverse side if necessary and identify by block number)

computations	Ludwieg tube	expansion
boundary layer	transonic flow	wave
growth	wind tunnels (pilot)	
measurement	Reynolds number	

20. ABSTRACT (Continue on reverse side if necessary and identify by block number)

Experimental boundary-layer measurements obtained in a Ludwieg tube used to drive a pilot transonic tunnel were compared with values calculated by a procedure developed by E. Becker and with those calculated by a method containing several modifications to Becker's method. The modifications fall into three general categories: the use of a skin-friction law and velocity profile exponent which are more accurate at high Reynolds numbers;

DD FORM 1 JAN 73 1473 EDITION OF 1 NOV 65 IS OBSOLETE

UNCLASSIFIED

20. ABSTRACT (Continued)

treatment of the momentum equation as axisymmetric instead of two-dimensional; and calculation at a specified location other than at the origin of the centered expansion wave. Inasmuch as these modifications greatly improved the agreement with experimental values, they are presented herein.

AFSC
Arnold AFS Tenn

PREFACE

The work reported herein was conducted by the Arnold Engineering Development Center (AEDC), Air Force Systems Command (AFSC), under Program Element 65807F. This work was done by ARO, Inc. (a subsidiary of Sverdrup & Parcel and Associates, Inc.), contract operator of AEDC, AFSC, Arnold Air Force Station, Tennessee. The research was conducted under ARO Project Numbers VF409 and V37A-32A. The author of this report was James C. Sivells, ARO, Inc. The manuscript (ARO Control No. ARO-VKF-TR-75-44) was submitted for publication on April 17, 1975.

The author wishes to acknowledge the assistance of Messrs. R. F. Starr and J. H. Porter, Jr., ARO, Inc., for providing the experimental data used in the comparisons with calculated results contained in this report.

CONTENTS

ILLUSTRATIONS

APPENDIX

1.0 INTRODUCTION

In a wind tunnel driven by a Ludwieg tube (Ref. 1), the air in the wind tunnel and tube is initially compressed to a desired charge pressure. Flow is initiated by breaking a diaphragm, or quickly opening a valve, located downstream of the test section. As the air is released, an expansion wave is created and travels upstream to the closed end of the tube where it is reflected and returned to the contraction section at the downstream end. Due to viscous effects in the airflow generated by the expansion wave, a boundary layer is formed whose thickness increases with time. During this excursion of the expansion wave, the stagnation pressure of the central core of flow through the wind tunnel is essentially constant until the thickness of the boundary layer at the downstream end of the tube approaches the radius of the tube. Thus, the useful run time for the Ludwieg tube wind tunnel depends upon the initial air temperature which determines the velocity of the head of the expansion wave, the length of the tube which is traversed by the expansion wave, and the diameter of the tube which determines the velocity of the airflow and relative to which the boundary-layer thickness eventually becomes critical.

Shortly after the conception of the tube wind tunnel, calculations of the growth of the boundary layer were made by E. Becker, (Refs. 2 and 3). Values calculated by Becker's method, however, considerably underestimated the boundary-layer thicknesses obtained experimentally in a pilot tunnel as shown in Fig. 1, which was presented in

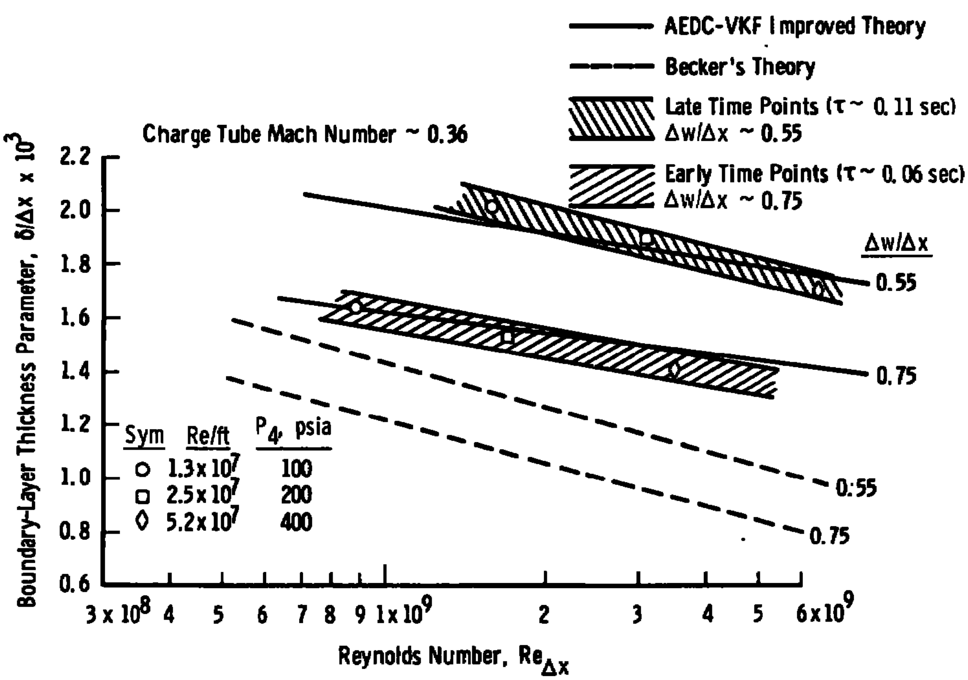

Figure 1. Charge tube boundary-layer thickness.

Ref. 4. In this figure, the Reynolds number is based on the distance Δx between the head of the expansion wave and the measuring station. Data are presented for two times, when the length of the expansion wave ΔW (head to tail) was about 55 and also about 75 percent of Δx. Three values of charge pressure P_4 are indicated.

Scrutiny of Becker's procedure indicated three categories in which modifications could be made to improve its correlation with the experimental data: the use of a skin-friction law and boundary-layer velocity-distribution which are more accurate at high Reynolds number; treatment of the momentum equation as axisymmetric instead of two-dimensional; and calculation at a specified location other than at the origin of the centered expansion wave. The latter is particularly important for a transonic wind tunnel utilizing a plenum chamber surrounding a porous-wall test section because the establishment of steady-state conditions in the test section determines when the tail of the expansion wave starts upstream through the Ludwieg tube.

When Becker's procedure was so modified, the results indicated as the AEDC-VKF improved method in Fig. 1 were obtained. The improvement in correlation with data from the pilot tunnel was considered to be sufficient to warrant the use of the modified method in any future applications.

2.0 THEORY OF OPERATION

The principle of operation can be described with the help of the wave diagram of Fig. 2. This diagram differs from the usual diagram which considers the diaphragm to be located at the downstream end of the tube. In the practical case of a transonic wind tunnel, the diaphragm or start valve is located downstream of the test section. When flow is initiated, the expansion wave travels upstream. The velocity of the head of the wave is the speed of sound a_o at the temperature of the charge air. The velocity of the air leaving the tube u_1 is determined by the ratio of the tube area to the area where the flow is sonic.

$$\frac{A_{tube}}{A^*} = \frac{1}{M_1}\left(\frac{2}{\gamma+1} + \frac{\gamma-1}{\gamma+1} M_1{}^2\right)^{\frac{\gamma+1}{2(\gamma-1)}} \tag{1}$$

and

$$M_1 = u_1/a_1 \tag{2}$$

The velocity of sound, a_1, in the air, after the flow is established, is related to a_o.

$$a_1/a_o = 1\Big/\left(1 + \frac{\gamma-1}{2} M_1\right) \tag{3}$$

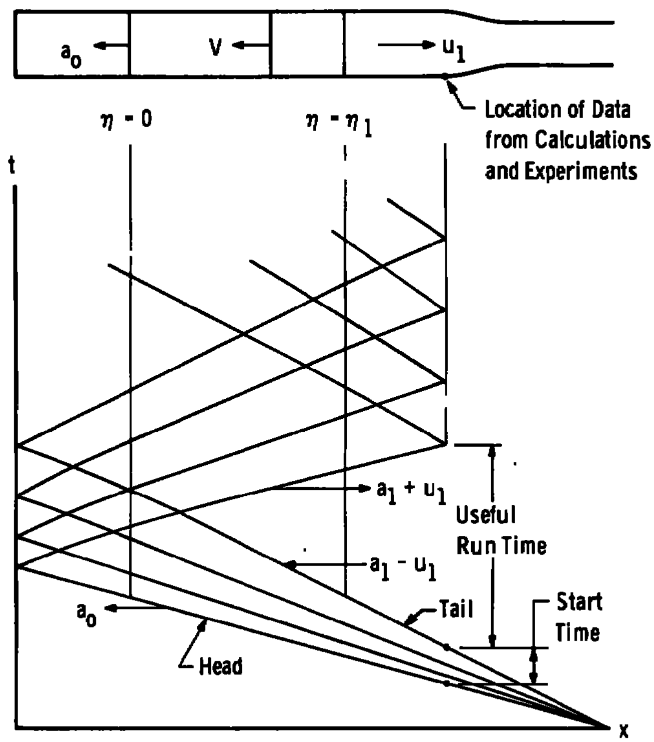

Figure 2. Characteristic diagram of expansion wave.

The velocity of the tail of the wave is $a_1 - u_1$; thus, the length of the expansion wave increases with time. The wave length is approximately linear with time after the wave is completely in the charge tube. For simplicity, it is also shown in Fig. 2 as linear downstream of the charge tube by extending the lines denoting the head and the tail of the wave until they meet at an effective location of the origin of the expansion wave. In the actual case of a porous-wall transonic test section, some time is spent in establishing steady-state conditions in the test section and plenum chamber. This in turn produces a noncentered wave process in the charge tube. The start time indicated in Fig. 2 is defined as the period of time during which the pressure at the end of the charge tube decreases from its charge value P_4 to the value of P_1 following the passage of the tail of wave, where

$$P_1/P_4 = (a_1/a_o)^{\frac{2\gamma}{\gamma - 1}} \tag{4}$$

From a knowledge of the start time, either from measurement or estimate, the effective time and position at which the wave length is zero can be determined.

In the development of the boundary-layer calculation, Becker solved the momentum equation twice: once for the growth of the boundary layer within the expansion wave and again for the growth of the boundary layer behind a fictitious concentrated wave of zero length moving at a velocity V intermediate between the velocities at the head and tail of the actual expansion wave. The value of this velocity was found by finding the distance behind the fictitious wave at which the boundary-layer thickness was the same as that at the tail of the expansion wave from the first solution. Becker introduced the variable η, where

$$\eta = 1 - \frac{x}{a_o t} \tag{5}$$

and η varies from 0 at the head of the expansion wave to η_1 at the tail and

$$\eta_1 = \frac{\gamma + 1}{2} M_1 \Big/ \left(1 + \frac{\gamma - 1}{2} M_1\right) \tag{6}$$

When Becker matched his boundary-layer solutions, he obtained a relation between V and u_1 (or a_o). When his relationship is expressed in a series on powers of η_1, it can be shown that

$$V/a_o = 1 - 2\eta_1/3 \tag{7}$$

is sufficiently accurate for practical values of η_1 up to about 0.45 and is independent of the choice of velocity profile exponent and friction coefficient law since these are contained only in the negligibly small coefficients of $\eta_1{}^2$ and higher powers of η_1. In the subsequent development of the modifications to improve the correlation of theory with experiment, it is assumed that this relationship, Eq. (7), is accurate inasmuch as only the flow behind the fictitious concentrated wave is considered.

3.0 MOMENTUM EQUATION

The time-dependent momentum equations for internal tube flow is adapted from Ref. 5 as

$$u_1 \frac{\partial}{\partial t} \int_0^\delta \left(1 - \frac{y}{r}\right) (\rho - \rho_1)\, dy + \frac{\partial}{\partial t} (\rho_1 u_1 \delta_1) + \frac{\partial u_1}{\partial y} \rho_1 u_1 \delta_1 + \frac{\partial}{\partial y} (\rho_1 u_1{}^2 \theta_1) = \tau_w \tag{8}$$

$$\delta_1 = \int_0^\delta \left(1 - \frac{y}{r}\right) \left(1 - \frac{\rho u}{\rho_1 u_1}\right) dy \tag{9}$$

$$\theta_1 = \int_0^\delta \left(1 - \frac{y}{r}\right) \frac{\rho u}{\rho_1 u_1} \left(1 - \frac{u}{u_1}\right) dy \tag{10}$$

$$\delta_1 = \delta^* - \delta^{*2}/2r \tag{11}$$

$$\theta_1 = \theta - \theta^2/2r \tag{12}$$

The quantities, δ_1 and θ_1, may be considered to be the displacement and momentum thicknesses when the boundary-layer thickness is small with respect to the radius of the tube. When the boundary-layer thickness is not small relative to the radius, the true values of δ^* and θ, obtained from mass-defect and momentum-defect considerations must be used to assess their effects on the flow but δ_1 and θ_1 are still used in Eq. (8). Becker did not use the $(1 - y/r)$ term in Eq. (8), (9), or (10), in which case Eq. (8) reduces to the two-dimensional form. In Ref. 1, Becker omitted the first term of Eq. (8). In Ref. 2, he included this term and also included the effects of compressibility and heat transfer on the ratio of ρ/ρ_1 within the boundary layer and upon the friction coefficient, and obtained essentially the same result (within about one percent) as for the incompressible case, at least for the usual conditions of operation of a Ludwieg tube.

The momentum equation can be simplified if it is assumed that the free-stream values of u_1 and ρ_1 are independent of time and a definition is added

$$\rho^* = \int_0^\delta \left(1 - \frac{y}{r}\right)\left(\frac{\rho}{\rho_1} - 1\right) dy \tag{13}$$

Also, in Eq. (8) the direction of x is positive in the direction u_1, but for the present purpose x is positive in the direction of wave propagation. Then

$$\frac{1}{u_1}\frac{\partial}{\partial t}(\rho^* + \delta_1) - \frac{\partial \theta_1}{\partial x} = \frac{\tau_w}{P_1 u_1^2} = \frac{C_f}{2} \tag{14}$$

It is assumed that the ratio $(\rho^* + \delta_1)/\theta_1$ is relatively independent of time. Then

$$\frac{\rho^* + \delta_1}{\theta_1 u_1}\frac{\partial \theta_1}{\partial t} - \frac{\partial \theta_1}{\partial x} = \frac{C_f}{2} \tag{15}$$

This equation can be integrated through the introduction of the distance $\underline{\overline{X}}$ defined as

$$\underline{\overline{X}} = Vt - x \tag{16}$$

which is the distance from the concentrated wave to the point x, and x and t are zero at the effective origin of the expansion wave. It is further assumed that the friction coefficient is a function of equivalent flat-plate momentum thickness, θ_c, such that

$$C_f/2 = d\,\theta_c/d\underline{\overline{X}} \tag{17}$$

In the absence of a longitudinal pressure gradient, Eq. (17) can be integrated to give

$$C_F/2 = \theta_c/\overline{X} \quad . \tag{18}$$

where the constant of integration is neglected. Eq. (15) can thus be integrated to give

$$\left(\frac{V}{u_1}\;\frac{\rho^* + \delta_1}{\theta_1} + 1\right)\theta_1 = \theta_c = \overline{X}\; C_F/2 = (Vt - x)\; C_F/2 \tag{19}$$

After rearranging

$$\theta_1 = \frac{(Vt - x)\, C_F/2}{1 + \frac{V}{u_1}\;\frac{\rho^* + \delta_1}{\theta_1}} \tag{20}$$

Finally,

$$\delta = \frac{\delta}{\theta_1}\;\frac{(Vt - x)}{1 + \frac{V}{u_1}\;\frac{\rho^* + \delta_1}{\theta_1}} \tag{21}$$

The ratios, δ/θ_1, ρ^*/θ_1, δ_1/θ_1, are obtained from Eqs. (9), (10), and (13) after the velocity and density distributions are assumed and

$$V/u_1 = (1/M_1) - (5 - \gamma)/6 \tag{22}$$

from Eqs. (2), (3), (6) and (7). The friction coefficient must be in a form which can be integrated with respect to the momentum thickness and must be corrected for at least first-order effects of compressibility and heat transfer. The heat transfer is from the wall to the air inasmuch as the mass of the wall is considered to be sufficient that its temperature is essentially constant during the short run time.

Except for the definition of the various parameters, the above derivation follows that of Becker. When $x = Vt$, i.e. at the location of the concentrated wave, the boundary-layer thickness is zero and increases, for a given value of t, as x decreases to zero. In the present treatment, the lowest value of t to be considered is the time required for the tail of the expansion wave to reach the downstream end of the charge tube and the value of x is the effective distance traveled by the wave tail. In Becker's evaluation of the boundary-layer parameters, he assumed that

$$u/u_1 = (y/\delta)^{1/7} \tag{23}$$

$$\frac{\rho - \rho_w}{\rho_1 - \rho_w} = \frac{u}{u_1} \tag{24}$$

$$C_{f_i} = 0.045\ Re_\delta^{-1/4} \tag{25}$$

and

$$C_{f_i}/C_f = F_c = \left(\frac{T_w + T_1}{2T_1}\right)^{1/2} \tag{26}$$

The accuracy of this choice of parameters is optimum for values of Re_δ of about 100,000 but deteriorates as the Reynolds number increases.

4.0 SKIN-FRICTION COEFFICIENT

One widely used expression for incompressible skin friction which correlates well with experimental data over a wide range of Reynolds numbers is that of von Kármán and Schoenherr (Ref. 6)

$$C_{f_i} = \frac{(0.242)^2}{(\log Re_{\theta_i} + 1.1696)(\log Re_{\theta_i} + 0.3010)} \tag{27}$$

which can be integrated to give the familiar

$$C_{f_i}^{1/2} = 0.242/\log(2\ Re_{\theta_i}) \tag{28}$$

Another expression (Ref. 7) is that based on Coles' law of the wall and law of the wake

$$\kappa\ (2/C_{f_i})^{1/2} = \ln Re_\delta + 0.5\ \ln\ (C_{f_i}/2) + \kappa C + 2\Pi \tag{29}$$

where the constants κ and C are 0.41 and 5.0, respectively, and Π is a function of Reynolds number and pressure gradient. If the laminar sublayer is neglected and the wake function is represented by a sine^2 distribution, integration of the profile gives

$$\frac{\delta_i^*}{\delta} = \frac{1 + \Pi}{\kappa}\left(\frac{C_{f_i}}{2}\right)^{1/2} \tag{30}$$

and

$$\frac{\theta_i}{\delta} = \frac{\delta_i^*}{\delta} \cdot \frac{C_{f_i}}{2\kappa^2}\ (2 + 3.179\ \Pi + 1.5\ \Pi^2) \tag{31}$$

Equations (30) and (31) must be used with Eq. (29) to determine C_{f_i} as a function of Re_{θ_i}. It may be noted that for an earlier version of the wake distribution (Ref. 8), the coefficients of Π and Π^2 in Eq. (31) were 3.2 and 1.522, respectively.

In order to use Eq. (29), values of Π must be known as a function of Reynolds number, even for the zero pressure gradient condition assumed herein. For the wake distribution used in Ref. 8, Coles found that Π seemed to have a constant value of 0.55 for values of Re_{θ_i} greater than about 6,000. For the sine^2 distribution used to obtain Eq. (31), the value of Π must be increased slightly to about 0.56 at Re_{θ_i} = 5,000 and further to about 0.58 at Re_{θ_i} = 29,000 in order to match the tabulated values of C_{f_i} therein. Even if Eq. (29) could be put into a form which could be integrated, the question arises as to how Π varies with Reynolds number to values about three orders of magnitude higher than that considered by Coles. Such large Reynolds numbers would be encountered in a large Ludwieg tube. Even the high Reynolds numbers of the experimental values of Kempf (Ref. 9) are about two orders of magnitude too low for comparison with a large Ludwieg tube.

If it is assumed that both Eqs. (27) and (29) give identical results and Eq. (31) is used to relate Re_{θ_i} with Re_δ, values of Π can be calculated by an iterative method. The results are shown in Fig. 3 and indicate an increasing value of Π with increasing Reynolds number.

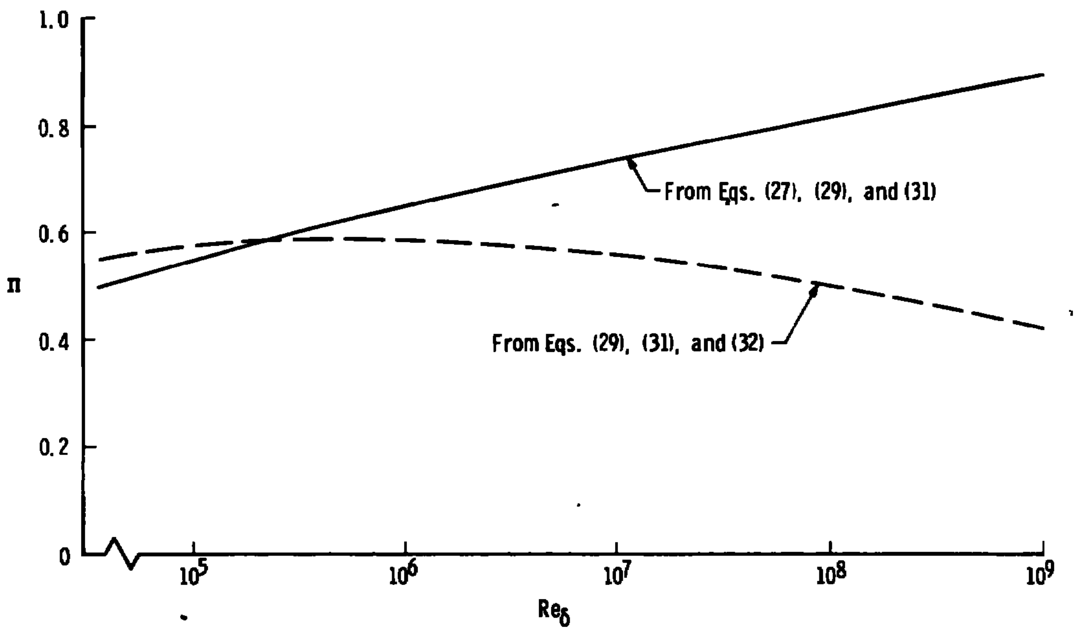

Figure 3. Variation of Π with Reynolds number.

A third expression for skin-friction coefficient used in Ref. 10* is

$$C_{f_i} = \frac{0.0773}{(\log Re_{\theta_i} + 4.561)(\log Re_{\theta_i} - 0.546)} \qquad (32)$$

*Constant 4.561 in Eq. (32) was 4.563 in Eq. (70) of Ref. 10.

which can be integrated to give

$$C_{F_i} = \frac{0.0773}{(log\ Re_{\theta_i} + 4.0895)\ (log\ Re_{\theta_i} - 0.9431)} \tag{33}$$

Equations (32) and (33) have been found to correlate well with available data. Equation (32) agrees almost exactly with Coles' tabulated values for Re_{θ_i} from 4,000 to 29,000. It gives values about two percent less than Eq. (27) at Re_{θ_i} = 500, the same as Eq. (27) at Re_{θ_i} = 23,300, and about six percent greater at Re_{θ_i} = 20,000,000. If Π is calculated from Eqs. (32), (29), and (31), the other curve in Fig. 3 is obtained. In this case, Π has a maximum value of about 0.5885 at Re_δ about 52,000 and decreases at higher Reynolds numbers. Although the value of C_{F_i} from Eq. (33) is less than two percent greater than that from Eq. (28) at the highest Reynolds number of Kempf's data, it is believed that further extrapolation by Eq. (32) is better than that by Eq. (27) and therefore Eqs. (32) and (33) are used hereinafter. For obtaining the ratio of θ_i/δ, the combination of Eqs. (32), (29), and (31) is used.

In Fig. 4, the limited range of application of Eq. (25) is clearly shown in comparison with Eq. (32) or even (27).

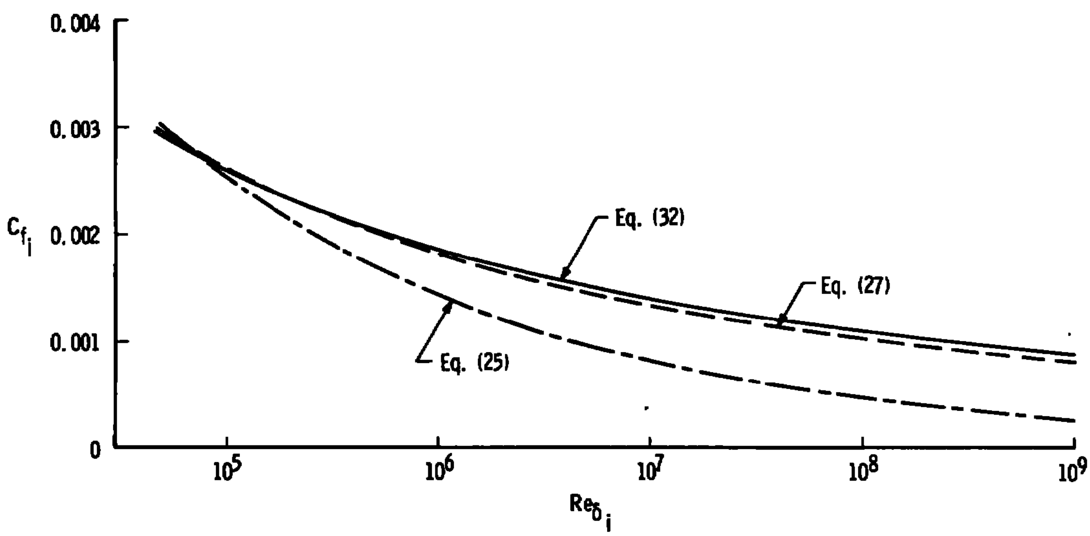

Figure 4. Comparison of incompressible skin-friction relations.

Conversion of the incompressible skin friction coefficient to the compressible value with heat transfer uses the concept that the value F_cC_f (or F_cC_F) is a function of F_{R_δ} Re_{θ_c} in the same manner that C_{f_i} (or C_{F_i}) is a function of Re_{θ_i}. The factor F_c used herein is that used by Spalding-Chi (Ref. 11) and Van Driest (Ref. 12)

$$F_c = [\int_0^1 (\rho/\rho_1)^{1/2}\ d(u/u_1)]^{-2} \tag{34}$$

where $\rho/\rho_1 = T_1/T$ within the boundary layer inasmuch as the static pressure in the boundary layer is assumed to be constant. The temperature distribution in the boundary layer is assumed to be the quadratic

$$\frac{T}{T_1} = \frac{T_w}{T_1} + \frac{(T_{aw} - T_w)}{T_1}\frac{u}{u_1} - \left(\frac{T_{aw}}{T_1} - 1\right)\left(\frac{u}{u_1}\right)^2 \tag{35}$$

where

$$T_{aw}/T_1 = 1 + r(\gamma - 1)M_1^2/2 \tag{36}$$

After substitution and integration, Eq. (34) becomes

$$F_c = \frac{(T_{aw}/T_1) - 1}{(\sin^{-1}\alpha + \sin^{-1}\beta)^2} \tag{37}$$

where

$$\alpha = \frac{T_{aw} + T_w - 2T_1}{[T_{aw} + T_w)^2 - 4T_1 T_w]^{1/2}} \tag{38}$$

and

$$\beta = \frac{T_{aw} - T_w}{[(T_{aw} + T_w)^2 - 4T_1 T_w]^{1/2}} \tag{39}$$

The factor F_{R_δ} used herein is that suggested by Van Driest

$$F_{R_\delta} = \mu_1/\mu_w \tag{40}$$

and Sutherland's viscosity law is used. These factors, F_c and F_{R_δ}, have been used for correlation at supersonic speeds with good results and should be satisfactory at the relatively low speed and heat transfer within the Ludwieg tube.

An additional factor which needs to be established is the velocity distribution in the boundary layer so that Eqs. (9), (10), and (13) can be evaluated. For simplicity, the power-law velocity distribution is assumed

$$\frac{u}{u_1} = \left(\frac{y}{\delta}\right)^{1/n} \tag{41}$$

where n is a function of Reynolds number and increases with increasing Reynolds number. If a kinematic momentum thickness is defined as

$$\theta_k = \int_0^\delta \frac{u}{u_1}\left(1 - \frac{u}{u_1}\right) dy \tag{42}$$

then

$$\theta_k/\delta = n/(n^2 + 3n + 2) \tag{43}$$

The best correlation with data was found if it were assumed that the value of n is a function of Reynolds number based on the actual boundary thickness, not corrected by F_{R_δ}, and θ_k/δ given by Eq. (31) with Π evaluated from Eqs. (29) and (32) with θ_k used instead of θ_i. Then

$$n = \frac{1}{2}\left\{\frac{\delta}{\theta_k} - 3 + \left[\left(\frac{\delta}{\theta_k} - 3\right)^2 - 8\right]^{1/2}\right. \tag{44}$$

Values of n evaluated in this manner are shown in Fig. 5.

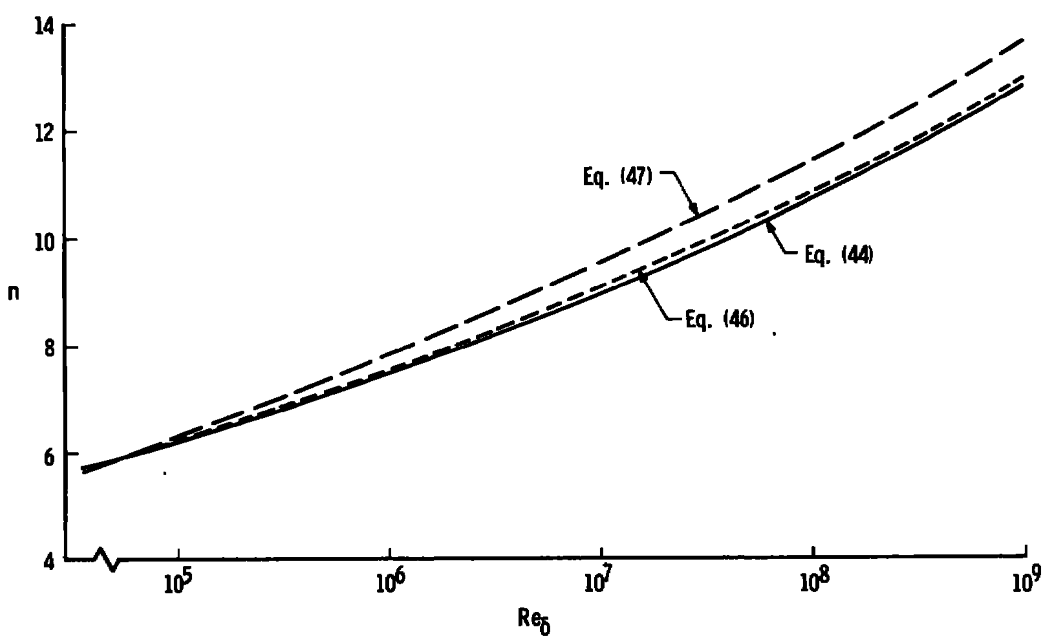

Figure 5. Variation of n with Reynolds number.

If a kinematic displacement thickness is defined as

$$\delta_k^* = \int_0^\delta \left(1 - \frac{u}{u_1}\right) dy \tag{45}$$

other definitions of n could be made

$$n = \frac{\delta}{\delta^*_k} - 1 \tag{46}$$

or

$$n = \frac{\delta}{\delta^*_k/\theta_k - 1} \tag{47}$$

The three definitions of n give the same value at an Re_δ of about 50,000, but the value defined by Eq. (47) is about six percent higher than that defined by Eq. (44) at Re_δ of 10^9. Inasmuch as Π is evaluated from the ratio θ_k/δ, it seems more logical to also evaluate n from the same ratio, and, in fact, Eq. (44) does seem to produce better correlation with experimental data.

5.0 CALCULATION PROCEDURE

The computer program for calculating the boundary-layer growth is given in Appendix A. A design Mach number in the Ludwieg tube is assumed and used to obtain an inviscid sonic area from Eq. (1). It is assumed that the boundary layer at the sonic area location is related to the boundary layer at the end of the Ludwieg tube by streamlines within the boundary layer. Along each of these streamlines, constant total pressure and temperature (enthalpy) are assumed which vary from streamline to streamline as determined from the assumed distributions of velocity and temperature within the boundary layer at the end of the Ludwieg tube. The resulting distributions can be integrated to give a displacement thickness which reduces the effective sonic area as well as the area in the Ludwieg tube. The Mach number in the Ludwieg tube thereby varies slightly with time inasmuch as the "viscid" area ratio differs from that assumed initially.

The earliest time for which calculations are made is the "start" time previously defined in Fig. 2. As a first approximation, the design Mach number is used to determine the pressure, temperature, velocities, and corresponding unit Reynolds number. Because C_F is based upon Re_{θ_c} and n is based upon Re_δ, successive approximations are made until a consistent set of values are determined to solve Eq. (21) for δ and to obtain the corresponding values of displacement thickness both at the end of the Ludwieg tube and at the sonic area location. From the latter, a second approximation for Mach number is obtained and the process is repeated. Usually about five complete approximations are needed to make the Mach number consistent with the "viscid" area ratio.

From the final calculation for the "start" time, the effective location of the origin of the expansion wave is determined for use in the calculations for later times. For the later times, calculations are made both at the tail of the wave and at the end of the charge tube. In the solution of the momentum equation, it was assumed that certain variables were constant, but, in actuality, there is some variation along the tube. Therefore, at the end of the charge tube, the denominator of Eq. (20) is the arithmetic average between that at the tail of the wave and that at the end of the charge tube. Approximations are made until the Mach numbers at the tail of the wave and at the end of the tube are consistent with the "viscid" area ratios at the corresponding locations. For each approximation, it is assumed that the Mach number at the tail of the wave determines the stagnation pressure in the tube, but the Mach number at the end of the tube determines the static pressure at the end of the tube. Again, about five or six approximations are needed to achieve consistency.

Obviously, the maximum value of δ is the radius of the charge tube. The calculated time at which this condition first occurs is the maximum time for the particular Ludwieg tube design even though the reflected expansion wave may not have returned to the downstream end of the tube. If there were no boundary layer, the pressures within the tube would be constant during each excursion of the expansion wave up and back down the tube. In actuality, the static pressure at the downstream end of the tube decreases with time. This decrease becomes greater as the design Mach number in the tube is increased. A phenomenon, reported by Piltz in Ref. 13 and qualitatively supported by calculations made by Piltz and by the method described herein, is that the stagnation pressure which initially decreases slightly with time may increase slightly at later times at design Mach numbers above about 0.2 but continues to decrease at lower design Mach numbers. The magnitude of these decreases and increases is a fraction of one percent of the theoretical inviscid values. After the boundary-layer thickness becomes equal to the tube radius, the stagnation pressure decreases more rapidly at first and less rapidly later as the boundary layer adjusts to the velocity profile of fully developed tube flow. Such behavior can be seen only if the Ludwieg tube is sufficiently long. From a practical standpoint, it would not be economical to build a Ludwieg tube with a run time greater than that which would allow the boundary-layer thickness to become nearly equal to the tube radius.

6.0 COMPARISON WITH EXPERIMENT

The comparison shown in Fig. 1, which was taken from Ref. 4, was made before the method described herein was developed to its present form, primarily in the realm of the variation of n with Reynolds number and the incorporation of the stream tube method of changing the effective sonic area with time. A comparison is made in Fig. 6 of the same experimental values with values calculated as described herein. Two sets of calculated values are shown to illustrate the sensitivity of the method to changes in start time and run time. One set of values uses the same start time of 0.032 sec for each pressure level together with run times of 0.060 and 0.110 sec. Curves drawn through these values indicate a greater influence of Reynolds number on boundary-layer thickness than that shown in Fig. 1 and, therefore, agree somewhat better with the experimental values. Moreover, the bands of the experimental data indicate the inaccuracies and spread of the data from many runs. The times for the second set of calculated points in Fig. 6 were selected so that the points for the lower and higher charge pressures lie more nearly in the center of the experimental bands in the manner of the points for the medium pressure. Only small changes in the times were necessary to produce the changes in boundary-layer thichness. These slight time variations which produce improved agreement are well within the experimental uncertainty.

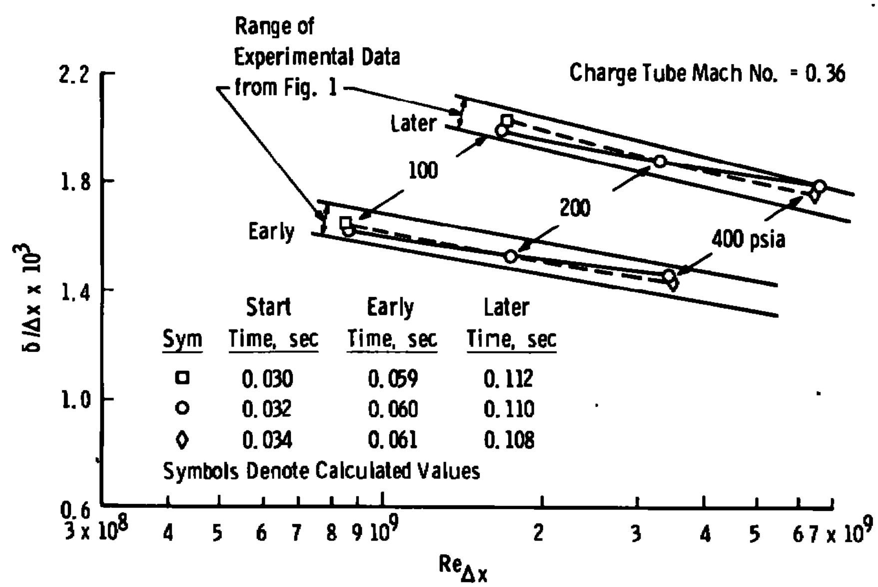

Figure 6. Comparison of calculated and experimental results for 11.75-in.-diam Ludwieg tube, revision of Figure 1.

The discussion above illustrates what the dangers may be in attempting to extrapolate experimental data to other sizes and operating conditions without an adequate theoretical method as a backup. The length of the Ludwieg tube used was insufficient to give values of δ greater than about one-half of its radius. The agreement between calculated and experimental results in the 7.6-percent scale pilot tunnel indicate that the present method would be adequate for application to the design of a full-scale facility. Data from charge tubes of 11.75- and 13.94-in. diameter were obtained.

Relatively few boundary-layer data were obtained at the downstream end of the larger charge tube. These are compared with calculated values in Figs. 7 and 8. The full boundary-layer thickness, δ, (Fig. 7) is predicted quite accurately. Close to the wall, however, the mass-flow profile (Fig. 8) is underestimated by the calculations, but beyond about 0.5 in. the agreement becomes much better. Because of the profile deviations, the values of displacement or momentum thickness are not quite as accurately predicted as the full thickness.

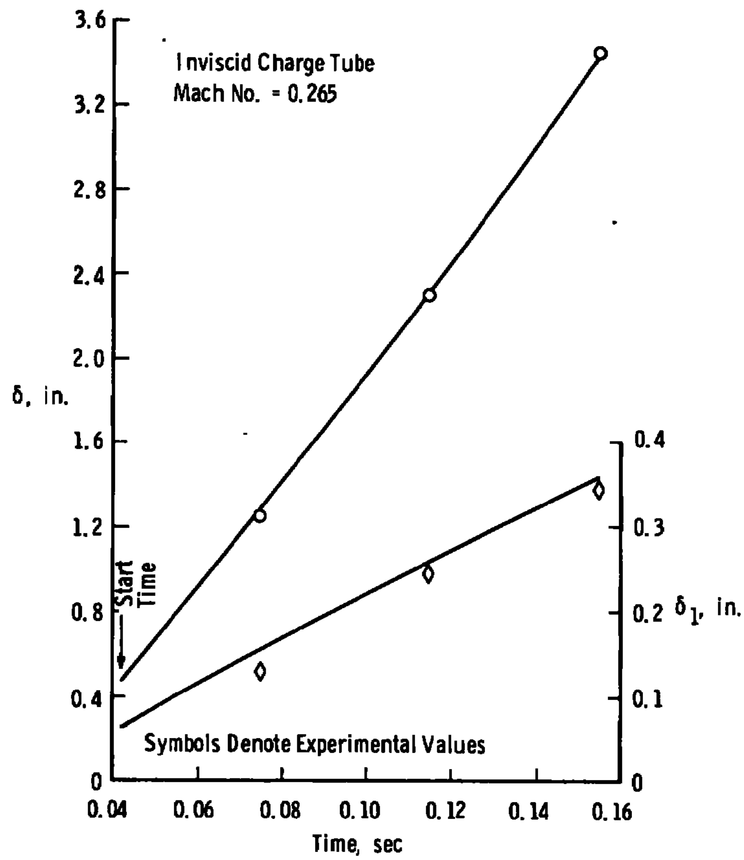

Figure 7. Comparison of calculated and experimental results for 13.94-in.-diam Ludwieg tube.

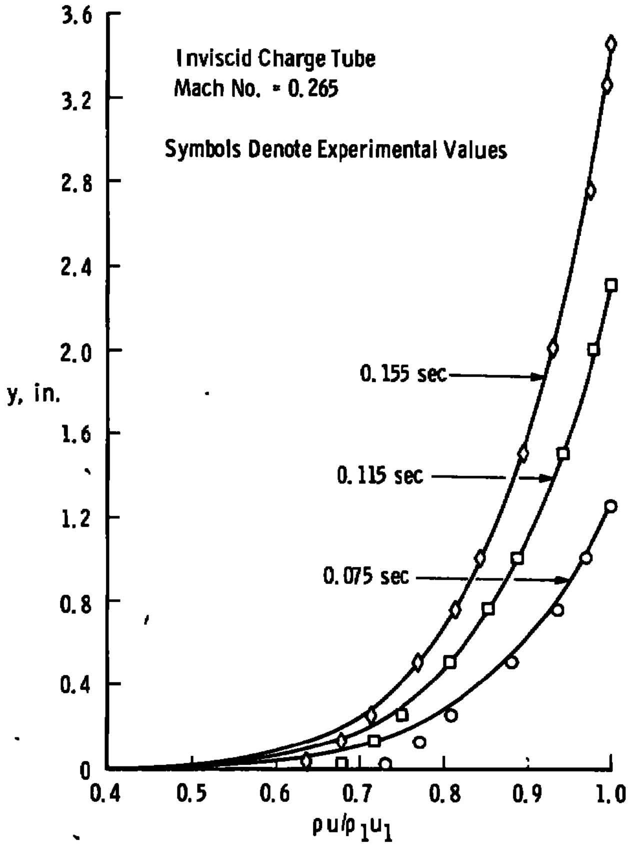

Figure 8. Calculated and experimental mass flux profiles in the 13.94-in.-diam Ludwieg tube.

For the range of Mach numbers under consideration, an error of 0.5 percent in measured pressure ratio will result in an error of nearly five percent in Mach number near the edge of the boundary layer and an error of nearly ten percent in Mach number at a point in the boundary layer where the Mach number is about 70 percent of the free-stream value. Thus, the deviations between calculated and experimental profiles are within the accuracy of the experimental values.

7.0 CONCLUDING REMARKS

A method is presented for calculating the time-dependent growth of the boundary layer at the downstream end of a Ludwieg tube. The method consists mainly of several modifications to Becker's method which had been found to be inadequate for use at high Reynolds numbers. Calculations made by the modified and improved method have been found to agree quite satisfactorily with experimental data obtained in a Ludwieg tube used to drive a small transonic tunnel. Utilizing the program developed in this study, very reliable predictions of the boundary-layer growth in the charge tube for wide range performance are possible.

REFERENCES

1. Ludwieg, H. Tube Wind Tunnel. "A Special Type of Blowdown Tunnel." AGARD Report 143, July 1957.

2. Becker, E. "Das Anwachsen der Grenzschicht in und hinter einer Expansionswelle." Ingenieur-Archiv, Vol. 25, 1957.

3. Becker. E. "Reibungswirkungen im Rohrwindkanal." Mitteilungen aus dem Max-Planck-Institute für Strömungsforchung und der Aerodynamischen Versuchsanstalt, Nr. 20, Göttingen, 1958.

4. Starr, R. F. and Schueler, C. J. "Experimental Studies of a Ludwieg Tube High Reynolds Number Transonic Tunnel." AEDC-TR-73-168 (AD771646), December 1973. Also Available as Paper No. 73-212 presented at AIAA 11th Aerospace Sciences Meeting, Washington, D.C., January 1973.

5. Young, A. D. "Boundary Layers. Modern Developments in Fluid Dynamics, High Speed Flow." Edited by L. Howarth, Vol. I, Chapter X, Oxford at the Clarendon Press, 1953.

6. Locke, F. W. S., Jr. "Recommended Definition of Turbulent Friction in Incompressible Fluids." DR Rep. 1415, Navy Department, Bureau of Aeronautics, Research Division, June 1952.

7. Coles, Donald E. "The Young Person's Guide to the Data." Proceedings AFOSR-IFP-Stanford 1968 Conference on Turbulent Boundary Layer Prediction. Vol. II, Edited by D. E. Coles and E. A. Hirst.

8. Coles, Donald E. "The Turbulent Boundary Layer in a Compressible Fluid." Rand Corporation Report. R-403-PR, 1962.

9. Kempf, von Gunther. "Neue Ergebnisse der Widerstandsforschung." Werft, Reederi, Hafen. Vol. 10, No. 11, pp. 234-239, No. 12, pp. 247-253, 1929.

10. Sivells, James C. Aerodynamic Design of Axisymmetric Hypersonic Wind Tunnel Nozzles. Journal of Spacecraft and Rockets, Vol. 7, No. 11, November 1970, pp. 1292-1299.

11. Spalding. D. B. and Chi, S. W. "The Drag of a Compressible Turbulent Boundary Layer on a Smooth Flat Plate With and Without Heat Transfer." Journal of Fluid Mechanics, Vol. 18, Part 1, January 1964, pp. 117-143.

12. Van Driest, E. R. "The Problem of Aerodynamic Heating." Aeronautical Engineering Review, Vol. 15, No. 10, October 1956, pp. 26-41.

13. Piltz, Eckart. "Boundary-Layer Effects on Pressure Variations in Ludwieg Tubes." AIAA Journal, Vol. 10, No. 8, August 1972, pp. 1095-1097.

APPENDIX A
COMPUTER PROGRAM

This Appendix contains a program listing together with a sample output of calculated results. The computer program is written in double precision Fortran IV for use with the IBM 370/165 Computer. It closely follows the description given in Calculation Procedure. Numerical integration is accomplished through the use of a 16-point Gaussian formula for the interval 0 to 1. To avoid the problem of infinite slopes when y/δ is the independent variable, the velocity ratio is made the independent variable, because, from Eq. (41)

$$y/\delta = (u/u_1)^n \quad \text{(A-1)}$$

and

$$d(y/\delta) = n(y/\delta)d(u/u_1)/(u/u_1) \quad \text{(A-2)}$$

In the program u/u_1, written in the output as U/UE, is the variable Z(K) and the D(K)'s are the corresponding weighting factors for the Gaussian integration. One subroutine, FMR, is used to determine the Mach number for a radius ratio.

Four cards supply the input data for a particular problem. The first card contains the title (ITLE) information in columns 2 through 12. On the other three cards, the format allows ten columns for each variable.

<u>Second Card</u>

Input	Columns	
GAM	1 - 10	Ratio of specific heats, γ
AR	11 - 20	Gas constant, ft^2/sec^2R
ZO	21 - 30	Compressibility factor, 1
RO	31 - 40	Recovery factor, r
VISC	41 - 50	Constant in viscosity law
VISM	51 - 60	Constant in viscosity law, viscosity = $VISC(T)^{1.5}/(T + VISM)$

Third Card

AKAT	1 - 10	Variable used if more than one problem is input at same time, see card A-290
CMACH	11 - 20	Design Mach number, if not specified, maximum value is calculated from the radius ratio, PP/RSTAR
PP	21 - 30	Radius (in.) of Ludwieg tube
RSTAR	31 - 40	Effective radius (in.) of test section or, if CMACH = 0, of sonic area; if RSTAR = 0, RSTAR is set equal to sonic radius calculated from CMACH
PPQ	41 - 50	Charge pressure, P_4, psia
TQ	51 - 60	Charge temperature, Rankine
TMIN	62 - 70	Start time, sec
BLD	71 - 80	If zero, boundary-layer profiles are not printed

Fourth Card

TM(K)	10 for each value of K	Times, seconds, at which calculations are desired; maximum value of K is 7; problem is terminated when TM(K) = 0

Output values, if not otherwise obvious

RE/IN	Reynolds number per inch in freestream
RTHI	Incompressible Reynolds number based on momentum thickness
FRD	$R_{\theta_i}/R_{\theta_c}$
FC	C_{Fi}/C_F
KCFI	1000 C_{f_i}
KCDI	1000 C_{F_i}
KCD	1000 C_F
TH	θ_1, in.

Y	R-DEL*A
M	Mach number at end of Ludwieg tube
D*2-D	$\int_0^\delta (1 - \rho u/\rho_1 u_1)dy$
DELTA*	δ_1, in.
DEL*A	δ^*, in.
H	δ_1/θ_1
R	Tube radius, r, in.
PO	Stagnation pressure, psia, at net time
PO0	Stagnation pressure, inviscid, at time 0
PE	Static pressure, psia, in freestream
PE0	Static pressure, inviscid, at time 0
TO	Stagnation temperature at net time
TAU*V	Distance to concentrated expansion wave from end of tube
XSTAR	Distance to end of tube from effective origin of expansion wave
HRH	ρ^*/θ_1
TAO	Distance to head of expansion wave from end of tube
DELAY TIME	Time required for head of expansion wave to reach end of tube from effective origin
V	Velocity of concentrated wave, fps
HSUM/VO	$(\rho^* = \delta_1)/\theta_1 u_1$ at tail of wave
HSUM/VE	At end of tube
THROAT	Values at RSTAR calculated from streamtube from end of Ludwieg tube to sonic area
TUBE	Length of Ludwieg tube for NET TIME for expansion wave travel from downstream end of tube to upstream end and return
NET TIME	Same as input TM(K); useful run time, Fig. 2, is NET TIME minus START TIME

```
C       PROGRAM LUDWIEG
C       BOUNDARY LAYER GROWTH IN LUDWIEG TUBE
        IMPLICIT REAL*8 (A-H,O-Z)
        COMMON /GG/ G1,G3,G5,G6,GA,RGA
        DIMENSION Z(16), D(16), ITLE(3), TM(8)
        ONE=1.D+0
        ZERO=0.0D+0
        D(1)=.0135762297D+0
        D(2)=.0311267620D+0
        D(3)=.0475792558D+0
        D(4)=.0623144856D+0
        D(5)=.0747979944D+0
        D(6)=.0845782597D+0
        D(7)=.0913017075D+0
        D(8)=.0947253052D+0
        Z(1)=.0052995325D+0
        Z(2)=.0277124885D+0
        Z(3)=.0671843988D+0
        Z(4)=.1222977958D+0
        Z(5)=.1910618778D+0
        Z(6)=.2709916112D+0
        Z(7)=.3591982246D+0
        Z(8)=.4524937451D+0
        DO 1 J=9,16
        D(J)=D(17-J)
1       Z(J)=1.D+0-Z(17-J)
2       READ (5,30,END=29) ITLE
3       READ (5,31,END=29) GAM,AR,ZO,RO,VISC,VISM
C       FOR GAMMA=1.4, G1=2.5, G3=1.5, G5=1/6, G6=5/6, G7=1.2, G8=0.2
C       GA=3, RGA=1/3, GM=0.4, GP=3.5
        GM=GAM-1.D+0
        G1=1.D+0/GM
        G8=.5D+0*GM
        G7=1.D+0+G8
        G6=1.D+0/G7
        G5=G8*G6
        GA=G1*G7
        G3=.5D+0*GA
        GP=GAM*G1
        RGA=GM*G6
4       READ (5,31,END=29) AKAT,CMACH,PP,RSTAR,PPQ,TQ,TMIN,BLD
C       RSTAR(HIRT)=60.5551805, RSTAR(PILOT HIRT)=4.62193583
        READ (5,31,END=29) (TM(K),K=1,8)
        MC=1.D+2*CMACH
        IRST=1.D+1*RSTAR
        IF ((MC.EQ.0).AND.(IRST.NE.0)) CMACH=FMR(PP/RSTAR,-1)
        WMN=CMACH
        OMACH=CMACH
        WRITE (6,40) ITLE,PPQ,TQ,TMIN,CMACH
        WRITE (6,33)
        YSTAR=PP*DSQRT(CMACH)/(G6+G5*CMACH**2)**G3
        IF (MC.EQ.0) YSTAR=RSTAR
        IF (IRST.EQ.0) RSTAR=YSTAR
        XRT=RSTAR/YSTAR
```

```
      SMACH=FMR(XRT,-1)
      AQ=DSQRT(GAM*AR*TQ)
      TW=TQ
      WMU=VISC*TW*DSQRT(TW)/(TW+VISM)
      IQ=0
      TIM=TMIN
      CAPI=.55D+0
5     TAO=12.D+0*TIM*AQ
      DLB=0.0D+0
      DLC=0.0D+0
      MA=0
6     IPP=0
      MA=MA+1
      TRS=1.D+0/(1.D+0+G8*OMACH)**2
      OBET=G8*OMACH**2
      STR=1.D+0/(1.D+0+OBET)
      TR=TRS/STR
      TO=TR*TQ
      PPS=PPQ*TR**GP
      IF ((IQ.EQ.0).AND.(MA.EQ.1)) PSO=PPS
      RHO=144.D+0*PPS/ZO/AR/TO
      TE=TO*STR
      EMU=VISC*TE*DSQRT(TE)/(TE+VISM)
      TAW=TE*(1.D+0+RO*OBET)
      RHOE=RHO*STR**G1
      AE=DSQRT(GAM*AR*TE)
      VE=OMACH*AE
      VO=OMACH*AE
      AT=AE-VO
      IF (TIM.GT.TMIN) GO TO 7
      QSEC=TMIN*AT/(AQ-AT)
      XST=AQ*QSEC
7     AV=(AQ+2.D+0*AT)/3.D+0
      TSEC=TIM+QSEC
      TAUV=12.D+0*TSEC*(AV-AT)
      REO=RHOE*VO/EMU/12.D+0
      KAT=0
      GO TO 9
8     IPP=0
      TAUV=12.D+0*(TSEC*AV-XST)
      PPE=PPS/(1.D+0+G8*WMN**2)**GP
      IF ((IQ.EQ.0).AND.(MA.EQ.1)) PEO=PPE
      BET=G8*WMN**2
      STR=1.D+0/(1.D+0+BET)
      TE=TO*STR
      TAW=TE*(1.D+0+RO*BET)
      RHOE=RHO*STR**G1
      EMU=VISC*TE*DSQRT(TE)/(TE+VISM)
      VE=WMN*DSQRT(GAM*AR*TE)
      REO=RHOE*VE/EMU/12.D+0
9     DW=TW/TE
      DA=TAW-TW
      DB=TAW-TE
      DK=DA/TE
```

```
      DN=DB/TE
      DC=DSQRT(DA*DA+4.0D+0*TW*DB)
      DF=DARSIN((DB+TW-TE)/DC)
      DE=DARSIN(DA/DC)
      TP=DB/(DF+DE)/(DF+DE)
      FRD=EMU/WMU
      XSTAR=TAUV/(1.D+0+1.3D+0*AV/VE)
      FC=TP/TE
      RXI=FRD*RED*XSTAR/FC
      IF (RXI.LT.1.D+2) GO TO 28
      AB=DLOG10(RXI)-1.5D+0
      RTHI=0.044D+0*RXI/AB**2
      RTII=RTHI
      RDEL=1.D+1*RTHI
10    IF (RTHI.LT.1.D+1) GO TO 27
      RTHG=DLOG10(RTHI)
      RTIG=DLOG10(RTII)
      CDI=0.03865D+0/(RTHG+4.0895D+0)/(RTHG-0.9431D+0)
      CFI=0.03865D+0/(RTIG+4.561D+0)/(RTIG-0.546D+0)
      XCF=.41D+0/DSQRT(CFI)
11    C2=1.D+0+CAPI
      C3=2.D+0+CAPI*(3.17897972D+0+1.5D+0*CAPI)
      C1=C2-C3/XCF
      FXCF=XCF+DLOG(C1)-1.1584018810+0-2.D+0*CAPI-2.302585093D+0*RTIG
      FPCP=(XCF-3.17897972D+0-3.D+0*CAPI)/XCF/C1-2.D+0
      CAPI=CAPI-FXCF/FPCP
      IF (DABS(FXCF).GT.1.D-8) GO TO 11
      DOTI=XCF/C1
      XN=.5D+0*(DOTI+DSQRT(DOTI*(DOTI-6.D+0)+1.D+0)-3.D+0)
      CD=CDI*TE/TP
      SUMA=0.0D+0
      SUMB=0.0D+0
      SUMC=0.0D+0
      SUMD=0.0D+0
      SUME=0.0D+0
      SMF=0.0D+0
      SMG=0.0D+0
      SMH=0.0D+0
      DO 12 K=1,16
      UN=Z(K)**XN
      TR=DW+Z(K)*(DK-Z(K)*DN)
      DD=D(K)*XN*UN
      ADD=DD/TR
      BDD=ADD*Z(K)
      CDD=ADD*UN
      DDD=BDD*UN
      SUMA=SUMA+ADD
      SUMB=SUMB+BDD
      SUMC=SUMC+CDD
      EDD=ADD/Z(K)
      HDD=EDD*UN
      SUME=SUME+EDD
      SMH=SMH+HDD
12    SUMD=SUMD+DDD
```

```
      DOT=1.D+0/(SUMA-SUMB)
      DSOD=1.D+0-SUMA
      DSM=0.5D+0-SUMC
      THM=SUMC-SUMD
      ROD=SUME-1.D+0
      RMD=.5D+0-SMH
      IF (IPP.GT.0) GO TO 13
      H=DSOD*DOT
      DOTR=DOT
      HRH=ROD*DOT
13    IF (KAT.EQ.0) GO TO 14
      HOVE=(H+HRH)/VE
      XSTAR=TAUV/(1.D+0+.5D+0*AV*(HOVO+HOVE))
      GO TO 15
14    HOVO=(H+HRH)/VO
      XSTAR=TAUV/(1.D+0+AV*HOVO)
15    TH=XSTAR*CD
      DOR=DOTR*TH/PP
      IF (DOR.LT.1.D+0) GO TO 16
      DOR=1.D+0
      TH=PP/DOTR
16    DSROD=DSOD-DOR*DSM
      DOTR=1.D+0/(1.D+0/DOT-THM*DOR)
      HR=DSROD*DOTR
      HRH=(ROD+DOR*RMD)*DOTR
      IF (DABS(H-HR).LT.5.D-7) GO TO 17
      H=HR
      IPP=1+IPP
      GO TO 13
17    DELTA=DOTR*TH
      IF (DOR.EQ.1.D+0) DELTA=PP
      RDLT=REO*DELTA
      RTHX=FRD*RDLT/DOT
      RTII=RDLT/DOTI
      DELST=HR*TH
      IF (DABS(1.D+0-RTHX/RTHI).LT.1.D-6) GO TO 18
      RTHI=RTHX
      RDEL=RDLT
      GO TO 10
18    IF (KAT.GT.0) GO TO 19
      OY=DSQRT(PP*(PP-2.D+0*DELST))
      KAT=1
      HO=H
      HRO=HRH
      XNO=XN
      GO TO 6
19    COLST=2.D+0*DELST/(DSQRT(1.D+0-2.D+0*DELST/PP)+1.D+0)
      DIFF=DABS(COLST-(2.D+0*DLB+DLC)/3.D+0)
      IF (DIFF.LT.1.D-6) GO TO 21
      FS=DSQRT(PP*(PP-2.D+0*DELST))
      TTR=BET*STR/G5
      DLC=DLB
      DO 20 K=1,16
      UN=Z(K)**XN
```

```
      TR=DW+Z(K)*(DK-Z(K)*DN)
      DD=D(K)*XN*UN
      UBR=DSQRT(TR-TTR*(TR-Z(K)**2))
      FDD=DD/UBR
      SMF=SMF+FDD
20    SMG=SMG+FDD*UN
      FFG=DSQRT((1.D+0-DOR)**2+2.D+0*DOR*(SMF-DOR*SMG))
      DLB=CDLST
      RX=PP*FFG/YSTAR
      DR=DY*RX/FS
      WMN=FMR(RX,-1)
      DMACH=FMR(DR,-1)
      GO TO 6
21    RTAO=REO*TAO
      DOL=DELTA/TAO
      DSOL=CDLST/TAO
      TRRX=XRT
      TMACH=SMACH
      IF ((IRST.EQ.0).OR.(MC.EQ.0)) FGG=FFG
      IF (BLD.EQ.0.0D+0) GO TO 23
      IF(MOD(IQ,2).NE.0) WRITE (6,41)
      WRITE (6,34)
      WRITE (6,35) ZERO,ZERO,ZERO,DW,ZERO
      DO 22 K=7,16
      UN=Z(K)**XN
      YBL=UN*DELTA
      TR=DW+Z(K)*(DK-Z(K)*DN)
      RHOU=Z(K)/TR
22    WRITE (6,35) UN,YBL,Z(K),TR,RHOU
      WRITE (6,35) ONE,DELTA,ONE,ONE,ONE
23    IF ((IRST.EQ.0).OR.(MC.EQ.0)) GO TO 25
      SMF=0.0D+0
      SMG=0.0D+0
      TBET=G8*TMACH**2
      TTT=BET*STR*(1.D+0+TBET)/TBET
      DO 24 K=1,16
      UN=Z(K)**XN
      TR=DW+Z(K)*(DK-Z(K)*DN)
      DD=D(K)*XN*UN
      UBR=DSQRT(TR-TTT*(TR-Z(K)**2))
      FDD=DD/UBR
      SMF=SMF+FDD
24    SMG=SMG+FDD*UN
      FGG=DSQRT((1.D+0-DOR)**2+2.D+0*DOR*(SMF-DOR*SMG))
      TRR=XRT*FFG/FGG
      TMACH=FMR(TRR,-1)
      IF (DABS(TRR-TRRX).LT.5.D-9) GO TO 25
      TRRX=TRR
      GO TO 23
25    DSBOR=1.D+0-(1.D+0-CDLST/PP)/FGG
      DBOR=1.D+0-(1.D+0-DOR)/FGG
      DW1=1.5D+0*(1.D+0-TAUV/TAO)
      THL=.5D+0*TRS*(TSEC*(AE+VO)+XST)-XST
      CDIK=2000.D+0*CDI
```

```
      CDK=2000.D+0*CD
      CFIK=2000.D+0*CFI
      DS2=DSOD*DELTA
      PSR=PPS/PSO
      PER=PPE/PEO
      WRITE (6,42) REO,RTHX,FRD,FC,CFIK,CDIK,CDK,TH
      WRITE (6,36) MA,FS,WMN,DELTA,DS2,DELST,CDLST,H,XN,PP,PPS,PPE,TO,TA
     1UV,XSTAR,HRH,OMACH,PSR,PER,TAO,QSEC,AV
      WRITE (6,43) XNO,HO,HRO,HOVO,HOVE,DWT
      WRITE (6,32) SMACH,TMACH,DSBOR,DBOR,TBL
      WRITE (6,39) RTAO,DOL,DSOL,TIM
      IQ=IQ+1
      TIM=TM(IQ)
      IF (TIM.LE.TMIN) GO TO 26
      IF ((BLD.EQ.0.0D+0).AND.(IQ.NE.5)) GO TO 5
      IF((BLD.NE.0.0D+0).AND.(MOD(IQ,2).NE.0)) GO TO 5
      WRITE (6,40) ITLE,PPQ,TQ,TMIN,CMACH
      WRITE (6,33)
      GO TO 5
26    IF (AKAT) 3,2,4
27    WRITE (6,37) RTHI,RDEL
      GO TO 29
28    WRITE (6,38) RXI,FRD,REO,XSTAR
29    STOP
C
30    FORMAT (3A4)
31    FORMAT (8E10.0)
32    FORMAT (1H ,10X,'INVISCID THROAT M=',F8.6,',  STREAMTUBE THROAT M=
     1',F8.6,',  DEL*A/RAD.=',F8.6,',  DELTA/RAD.=',F8.6,',  TUBE=',
     2F7.2,' FT.LG' / )
33    FORMAT (1H ,5X,'QUADRATIC TEMPERATURE DISTRIBUTION      SPAULDING-C
     1HI REFERENCE TEMPERATURE      VAN DRIEST REFERENCE REYNOLDS NO.' /)
34    FORMAT (1H0,10X,'Y/DELTA',10X,'Y(INCH)',11X,'U/UE',13X,'T/TE',11X,
     1'MASS FLUX' /)
35    FORMAT (1H ,5F17.5  )
36    FORMAT (1H ,'APPR',I3,',  Y=',F9.5,',  M=',F8.6,',  DELTA=',F9.5,
     1',  D*2-D=',F8.5,',  DELTA*=',F8.5,',  DEL*A=',F8.5,',  H=',F9.6,
     2',  N=',F8.5 ,/11X,'R=',F9.5,',  PO=',F8.3,',  PE=',F8.3,',  TO=',
     3F8.3,',  TAU*V=',F9.2,' IN.,  XSTAR=',F9.3,' IN.,  HRH=',F9.6/11X,
     4'WAVE END M=',F8.6,',  PO/POO=',F8.5,',  PE/PEO=',F8.5,',  TAO=',
     5F9.2,' IN.,  DELAY TIME=',F9.6,' SECONDS,  V=',F9.3 )
37    FORMAT (1H1,'RTHI=',E15.7,'RDEL=',E15.7 )
38    FORMAT (1H1,'RXI=',E15.7,'FRD=',E15.7,'REO=',E15.7,'XSTAR=',E15.7)
39    FORMAT (1H ,10X,'REYNOLDS NO.(TAO)=',1PE12.5,',  DELTA/TAO=',E12.5
     1,',  DEL*A/TAO=',E12.5,',  NET TIME=',0PF9.6,' SECONDS' / )
40    FORMAT (1H1,3A4,' CHARGE PRESSURE=',F7.2,' PSIA,  CHARGE TEMPERATU
     1RE=',F7.2,' R,  START TIME=',F9.6,' SECONDS,  DESIGN M=',F8.6 /)
41    FORMAT (1H0)
42    FORMAT (1H0,10X,'RE/IN=', F9.0,',  RTHI=',F9.0,',  FRD=',F8.6,',
     1FC=',F8.6,',  KCFI=',F8.5,',  KCDI=',F8.5,',  KCD=',F8.5,',  TH=',
     2F8.5 )
43    FORMAT (1H ,10X,'WAVE END N=',F8.5,',  H=',F9.6,',  HRH=',F9.6,',
     1 HSUM/VO=',F11.9,',  HSUM/VE=',F11.9,',  WAVE LGTH/TAO=',F7.5 /)
      END
```

```
      FUNCTION FMR (RR,IS)
C     TO OBTAIN MACH NUMBER FROM RADIUS RATIO, IS=-1 IF M<1, +1 IF M>1
      IMPLICIT REAL*8 (A-H,O-Z)
      COMMON /GG/ G1,G3,G5,G6,GA,RGA
      IF (RR.GT.1.D+0+5.D-10) GO TO 1
      FMR=1.D+0
      IF (RR.LT.1.D+0-5.D-10) GO TO 5
      RETURN
1     AB=(RR**2)**RGA
      IF (IS*AB.LT.-1.45D+0) GO TO 2
      FMR=(1.D+0+IS*DSQRT((AB-1.D+0)/G1))**GA
      GO TO 3
2     FMR=(G6**G3/RR)**2
3     DO 4 J=1,50
      CM=FMR**RGA
      FM=CM*AB-G6-G5*FMR**2
      FP=RGA*(CM*AB/FMR-FMR)
      FMR=FMR-FM/FP
      IF (DABS(FM).LT.1.D-9) GO TO 6
4     CONTINUE
5     RS=(G6+G5*FMR**2)**G3/DSQRT(FMR)
      WRITE (6,7) RR,FMR,RS
6     RETURN
C
7     FORMAT (1H ,'RADIUS RATIO=',F12.10,', M=',F12.10,7H, R/R*=,F12.10)
      END
```

SAMPLE INPUT

```
CARD 1
 ITLE
PILOT HIRT

CARD 2
 GAM        AR        ZO        RO        VISC        VISM
 1.4      1716.55     1.        0.896     2.2697E-8   198.72

CARD 3
 AKAT      CMACH      PP        RSTAR        PPQ      TQ       TMIN     BLD
  1.       .265      6.96875   4.62193583    102.     520.     .042     1.

CARD 4
 TM(1)     TM(2)     TM(3)     TM(4)     TM(5)     TM(6)     TM(7)
 .075      .115      .155
```

PILOT HIRT CHARGE PRESSURE= 102.00 PSIA, CHARGE TEMPERATURE= 520.00 R, START TIME= 0.042000 SECONDS, DESIGN M=0.265000

QUADRATIC TEMPERATURE DISTRIBUTION   SPAULDING-CHI REFERENCE TEMPERATURE   VAN DRIEST REFERENCE REYNOLDS NO.

Y/DELTA	Y(INCH)	U/UE	T/TE	MASS FLUX
0.0	0.0	0.0	1.11084	0.0
0.00082	0.00038	0.35920	1.07403	0.33444
0.00406	0.00191	0.45249	1.06392	0.42531
0.01526	0.00717	0.54751	1.05339	0.51976
0.04551	0.02139	0.64080	1.04282	0.61449
0.11142	0.05236	0.72901	1.03262	0.70598
0.22943	0.10783	0.80894	1.02319	0.79060
0.40426	0.18999	0.87770	1.01496	0.86477
0.61701	0.28998	0.93282	1.00826	0.92517
0.82273	0.38666	0.97229	1.00342	0.96897
0.96378	0.45295	0.99470	1.00066	0.99405
1.00000	0.46997	1.00000	1.00000	1.00000

RE/IN= 875318., RTHI= 36147., FRD=0.920584, FC=1.056867, KCFI= 2.07820, KCDI= 2.47275, KCD= 2.33970, TH= 0.04394
APPR 5, Y= 6.90503, M=0.269827, DELTA= 0.46997, D*2-D= 0.06461, DELTA*= 0.06343, DEL*A= 0.06372, H= 1.443554, N= 6.94305
R= 6.96875, PO= 74.266, PE= 70.602, TO= 474.929, TAU*V= 187.80 IN., XSTAR= 37.561 IN., HRH=-0.155787
WAVE END M=0.269827, PO/POO= 0.99538, PE/PEO= 0.99361, TAO= 563.41 IN., DELAY TIME= 0.094713 SECONDS, V= 888.925
WAVE END N= 6.94305, H= 1.443554, HRH=-0.155787, HSUM/VO=0.004499698, HSUM/VE=0.004499699, WAVE LGTH/TAO=1.00000

INVISCID THROAT M=0.955942, STREAMTUBE THROAT M=0.957060, DEL*A/RAD.=0.000965, DELTA/RAD.=0.059742, TUBE= 24.66 FT.LG

REYNOLDS NO.(TAO)= 4.93163D 08, DELTA/TAO= 8.34153D-04, DEL*A/TAO= 1.13102D-04, NET TIME= 0.042000 SECONDS

Y/DELTA	Y(INCH)	U/UE	T/TE	MASS FLUX
0.0	0.0	0.0	1.11178	0.0
0.00045	0.00057	0.35920	1.07480	0.33420
0.00254	0.00326	0.45249	1.06461	0.42503
0.01068	0.01369	0.54751	1.05399	0.51946
0.03497	0.04480	0.64080	1.04332	0.61419
0.09240	0.11839	0.72901	1.03301	0.70571
0.20237	0.25928	0.80894	1.02349	0.79038
0.37421	0.47945	0.87770	1.01515	0.86460
0.59212	0.75864	0.93282	1.00837	0.92507
0.80916	1.03671	0.97229	1.00347	0.96893
0.96075	1.23094	0.99470	1.00066	0.99404
1.00000	1.28122	1.00000	1.00000	1.00000

RE/IN= 897425., RTHI= 95738., FRD=0.919963, FC=1.057445, KCFI= 1.79908, KCDI= 2.11047, KCD= 1.99582, TH= 0.10958
APPR 5, Y= 6.81071, M=0.277158, DELTA= 1.28122, D*2-D= 0.16437, DELTA*= 0.15625, DEL*A= 0.15804, H= 1.425919, N= 7.53505
R= 6.96875, PO= 74.251, PE= 70.393, TO= 474.903, TAU*V= 539.48 IN., XSTAR= 109.808 IN., HRH=-0.155750
WAVE END M=0.270032, PO/POO= 0.99518, PE/PEO= 0.99067, TAO= 1006.09 IN., DELAY TIME= 0.094713 SECONDS, V= 888.760
WAVE END N= 7.05636, H= 1.439320, HRH=-0.155482, HSUM/VO=0.004482741, HSUM/VE=0.004322653, WAVE LGTH/TAO=0.69568

INVISCID THROAT M=0.955942, STREAMTUBE THROAT M=0.958898, DEL*A/RAD.=0.002565, DELTA/RAD.=0.167056, TUBE= 44.66 FT.LG

REYNOLDS NO.(TAO)= 9.02890D 08, DELTA/TAO= 1.27347D-03, DEL*A/TAO= 1.57086D-04, NET TIME= 0.075000 SECONDS

NOMENCLATURE

A^*	Sonic area
A_{tube}	Cross-section area of a Ludwieg tube
a_o	Speed of sound ahead of an expansion wave
a_1	Speed of sound behind an expansion wave
C	Constant in Eq. (29)
C_F	Mean skin-friction coefficient
C_f	Local skin-friction coefficient
F_c	Ratio of incompressible friction coefficient to compressible value
F_{R_δ}	$R_{\theta_i}/R_{\theta_c}$
ℓn	Denotes natural logarithm (base e)
log	Denotes common logarithm (base 10)
M	Mach number
n	Exponent in velocity profile
P_1	Static pressure behind expansion wave
P_4	Charge pressure
Re	Reynolds number, subscript indicates reference length
r	Radius of Ludwieg tube, also recovery factor in Eq. (36)
T	Temperature
t	Time
u	Velocity
V	Velocity of concentrated expansion wave
$\underline{\overline{X}}$	Distance, Vt-x

x	Distance along Ludwieg tube
y	Distance from wall of Ludwieg tube, in.
α	Variable defined by Eq. (38)
β	Variable defined by Eq. (39)
γ	Ratio of specific heats
Δx	Length traversed by head of expansion wave relative to end of Ludwieg tube
Δw	Length from head to tail of expansion wave
δ	Boundary-layer thickness
δ^*	Displacement thickness of boundary layer when total thickness is large relative to the tube radius
δ_1	Displacement thickness defined by Eq. (9)
δ_k	Kinematic displacement thickness, Eq. (45)
η	Nondimensional variable defined by Eq. (5)
θ	Momentum thickness of boundary layer when total thickness is large relative to tube radius
θ_1	Momentum thickness defined by Eq. (10)
θ_c	Equivalent flat-plate momentum thickness
θ_k	Kinematic momentum thickness, Eq. (42)
κ	Constant in logarithmic velocity profile
μ	Viscosity
Π	Wake variable in logarithmic velocity profile
ρ	Density
ρ^*	Density integral defined by Eq. (13)
τ_w	Shear stress at wall

SUBSCRIPTS

aw	Adiabatic wall value
i	Incompressible value
w	Wall value
1	Value behind expansion wave or outside of boundary layer, except δ_1 and θ_1